Supporting Information for

Modulating *Vibrio cholerae* Quorum-Sensing-Controlled Communication Using Autoinducer-Loaded Nanoparticles

Hoang D. Lu,[†] Alina C. Spiegel,[‡] Amanda Hurley,[§] Lark J. Perez,[Ψ] Katharina Maisel,[δ] Laura M. Ensign,[γ] Justin Hanes,[γ] Bonnie L. Bassler,[§,Φ] Martin F. Semmelhack,[‡] and Robert K. Prud'homme[†]*

Departments of [†]Chemical and Biological Engineering, [‡]Chemistry, and [§]Molecular Biology, Princeton University, Princeton, New Jersey 08544, United States; [Ψ]Department of Chemistry and Biochemistry, Rowan University, Glassboro, NJ 08028, United States; [δ]Department of Biomedical Engineering, and [γ]Center for Nanomedicine at the Wilmer Eye Institute, Department of Ophthalmology, Johns Hopkins University School of Medicine, Baltimore, MD 21218, United States; and [Φ]Howard Hughes Medical Institute, Chevy Chase, MD 20815, United States

*to whom correspondence should be addressed; E-mail: prudhomm@princeton.edu

Materials and Methods

Flash NanoPrecipitation and particle formation.

Nanoparticles were formed by rapidly mixing nanoparticle components dissolved in tetrahydrofuran against PBS using confined impingement jets as previously described.[1] 1.6 kDa polystyrene-block-5 kDa polyethylene glycol (PS-b-PEG) was used as the particle stabilizer (Polymer Source), and α-tocopherol (VitE) was used as the particle co-core (Sigma-Aldrich). CAI-1 was synthesized and purified as previously described.[2] When used, PS-b-PEG was dissolved at 10 mg mL^{-1}, VitE at 7.5 mg mL^{-1}, and CAI-1 at 7.5 mg mL^{-1}. Organic streams were

mixed with PBS at equal velocities and diluted ten-fold in PBS. Organic solvent was removed by reduced pressure at 60 torr for fifteen minutes. For dialysis experiments, nanoparticles were dialyzed in thousand-fold excess PBS through a 10 kDa MWCO membrane (Spectra/Por, Spectrum Labs) for three hours. For ultrafiltration experiments, nanoparticles were separated from PBS through a 30 kDa MWCO membrane (Amicon Ultra, Millipore) using 5,000g centrifugal force. Nanoparticles in the retentate were collected and resuspended to their original volume by the addition of fresh PBS, and nanoparticle-free PBS was collected from the ultrafiltration flow through.

Slow precipitation particle formation.

Particles were assembled via slow precipitation by dialyzing dissolved particle components against excess water through a 3.5 kDA MWCO membrane (Spectra/Por, Spectrum Labs) overnight. CAI-1 particles were formed by using PS-b-PEG dissolved at 10 mg mL^{-1}, VitE at 7.5 mg mL^{-1}, and CAI-1 at 7.5 mg mL^{-1} in THF. VitE particles were formed using PS-b-PEG dissolved at 10 mg mL^{-1} and VitE at 7.5 mg mL^{-1}.

Nanoparticle size and stability characterization.

Nanoparticle hydrodynamic diameters were determined by dynamic light scattering analysis (Malvern Zetasizer Nano, Malvern Instruments). Nanoparticles were diluted ten-fold into PBS, pH 2 PBS, LB medium, or 2% bile salts and incubated at 37°C for varying amounts of time. Sizes were measured using backscattering analysis with illumination from a helium neon laser at 632 nm. Buffers were filtered through 0.45 μM membranes to remove debris. Size spectra are intensity-weighted distributions.

Quorum-sensing activity determination and cell growth profiles.

The activity of CAI-1 was determined using bioluminescence from the *V. cholerae* WN1102 reporter strain [Δ*cqsA* Δ*luxQ*/pBB1] as previously described.[3] WN1102 was grown in LB broth containing 10 μg mL^{-1} tetracycline with shaking at 37°C overnight, and diluted to an OD_{600} of 0.13 (~twenty fold dilution) into the same medium. To each well in a black tissue-culture treated polystyrene plate (Corning) was added 150 μL of diluted cells. CAI-1 was serially diluted in DMSO, and 1.5 μL was added to culture wells to achieve the designated concentrations. Stock solutions of CAI-1 NPs were made and added to cells to the final noted concentrations, except CAI-1 NPs were serially diluted using PBS instead of DMSO. Serial dilutions of CAI-1 and PBS and VitE NPs were equivalently made using PBS, and added to cells in the same manner. Only the water soluble fraction of CAI-1 in PBS was used for experiments. Following addition of CAI-1, CAI-1

NPs, and VitE NPs, strain WN1102 was grown at 37°C for up to six hours with shaking. Cell growth and CAI-1 bioactivity were monitored by recording OD_{600} and bioluminescence (EnVision Multilabel Reader, PerkinElmer). Optical densities were corrected by subtracting background OD_{600} from preparations lacking cells. Bioluminescence units are counts per second per 150 µL culture. Reported data are averages and error bars are standard deviations of three separate well measurements.

Biofilm inhibition determination.

The ability of CAI-1 to inhibit adherent biofilms of *V. cholerae* WN1102 was determined with a modified crystal violet staining protocol.[4] WN1102 was grown in LB containing 10 µg mL^{-1} tetracycline at 37°C overnight with shaking, and diluted 100 fold into the same medium. Cells, CAI-1, and nanoparticles were added to 96 well plates as described above, mixed to homogeneity, and grown at 37°C overnight under static conditions. Plates were covered with an oxygen and carbon dioxide permeable medical grade polyurethane membrane to prevent well evaporation (BreatheEasy, Diversified Biotech). Non adherent cells were rinsed out of plates with DI water three times, and adherent biofilms were stained with 0.1% crystal violet. Unbound crystal violet was removed by rinsing with DI water three times, and bound crystal violet was solubilized by the addition of 30% acetic acid. Levels of solubilized crystal violet were determined by absorbance at 570 nm (Synergy Microplate Reader, Biotek). Measurements were normalized to biofilm production of WN1102 incubated with either DMSO or PBS containing no CAI-1. Values are averages and error bars are standard deviations of four separate well measurements.

***Ex vivo* particle tracking in intestinal mucus.**

Fluorescent CAI-1 nanoparticles were formed by encapsulating the hydrophobic dye Ettp5 within the nanoparticle core.[5] Particles were formed by flashing PS-b-PEG dissolved at 10 mg mL^{-1}, VitE at 7.5 mg mL^{-1}, CAI-1 at 7.5 mg mL^{-1}, and Ettp5 at 0.4 mg mL^{-1} in THF. Nanoparticles were extensively dialyzed against water prior to use for particle tracking experiments. Mice were starved overnight to reduce the amount of digestive material in the small intestine prior to *ex vivo* tracking, which was performed as previously described.[6] Briefly, the small intestine was excised, longitudinally sliced open, and a 1 cm segment of tissue was placed in a custom-made 0.5 x 1 cm chamber. A volume of 0.5 µL of nanoparticles was carefully pipetted on top of the mucus coating the tissue. The wells were then sealed by placing a cover slide on top of the tissue and affixing it using superglue, and the slides were imaged within 10 min of preparation. We have previously found that densely PEG-coated nanoparticles up to 210 nm in size rapidly penetrate murine small intestine mucus using these techniques.[6] Alternatively, 30 µL of simulated intestinal fluid (TS, Ricca Chemical) was added to a custom-made well. A

volume of 1 µL of nanoparticles was gently mixed into the fluid, and the well was sealed similarly with a cover slide affixed with super glue. Particle motions in simulated intestinal fluid and in mucus coating freshly excised murine small intestinal tissue were recorded using an Evolve 512 EMCCD camera (Photometrics) mounted on an inverted epifluorescence microscope (Axio Observer, Zeiss) with a 100X/1.46 NA objective and appropriate filter. Movies were collected for 20 s at a temporal resolution of 67 ms with Metamorph software (Molecular Devices). Movies were analyzed using automated particle tracking software custom-written in MATLAB to determine the x and y positions of particle centroids over time, as previously described.[7] The time-averaged mean square displacement (MSD) of each trajectory was calculated as previously described.[7, 8]

Supplemental background on quorum sensing and virulence suppression in *V. cholerae*

We briefly outline the issues involved in *V. cholerae* virulence in for readers unfamiliar with the field and refer the reader to in depth discussions in original references.[9-13] The discussion follows the presentation in Figure S1 adapted from Ng *et. al*.[14] The CAI-1 autoinducer is produced by the CqsA enzyme and released in the environment. CAI-1 binds to CqsS and modulates CqsS activity. At low cell density and low CAI-1 levels, CqsS possesses kinase activity, that phosphorylates the regulatory proteins LuxU and LuxO. Phosphorylated LuxU and LuxO leads to the transcription of quorum regulating RNA (Qrr) that represses HapR and elevates AphA expression, causing the upregulation of *vps* and *toxT*. Upregulated *vps* increases biofilm production, and upregulated *toxT* increases virulence factor production. In contrast, at high cell density and high CAI-1 levels, CqsS possesses phosphatase activity, and dephosphorylates LuxU. This leads to a cascade of events that result in the downregulation of *vps* and *toxT*, causing decreased biofilm production and decreased virulence factor production. There is also upregulation of *hap*, causing the production of detachment proteases that allow *V. cholerae* to separate itself from the small intestine and exit the host. Thus, CAI-1 may be used as a drug to treat cholera by simply modulating natural bacterial communication circuits.

Supplementary Figures

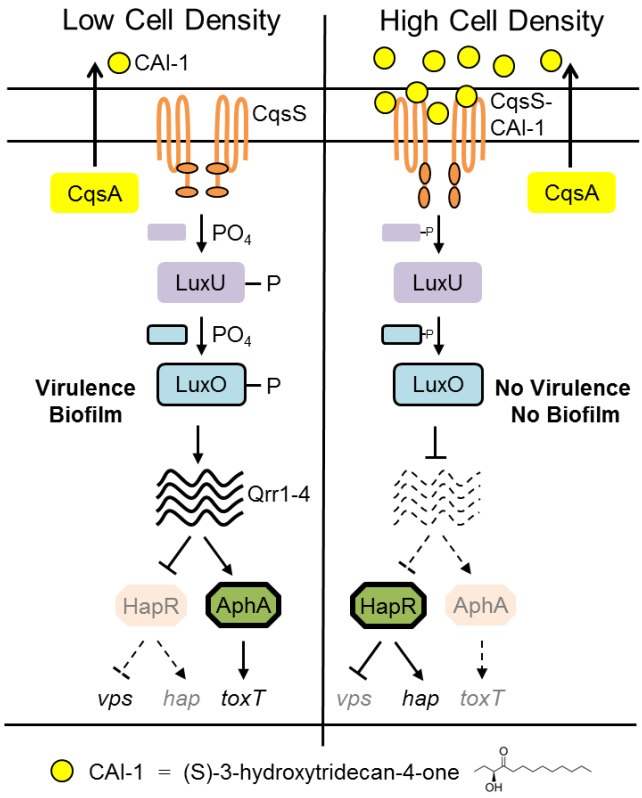

Figure S1. Basic quorum-sensing pathway in *V. cholerae* and mechanism of CAI-1 action. (Adapted with from Reference #14. Copyright (2012). PLOS)

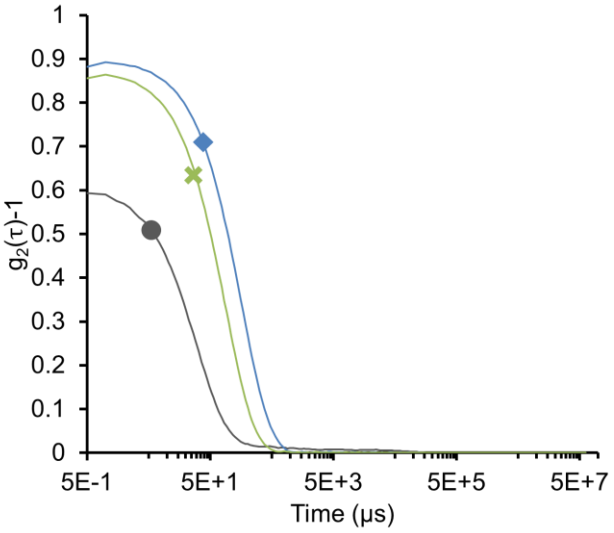

Figure S2. Flash NanoPrecipitation of CAI-1 nanoparticles. Dynamic light scattering correlation functions of CAI-1 NPs flashed with stabilizer, co-core, and CAI-1 (◆); of VitE NPs flashed with stabilizer and co-core (×); and of empty micelles flashed with only stabilizer (●).

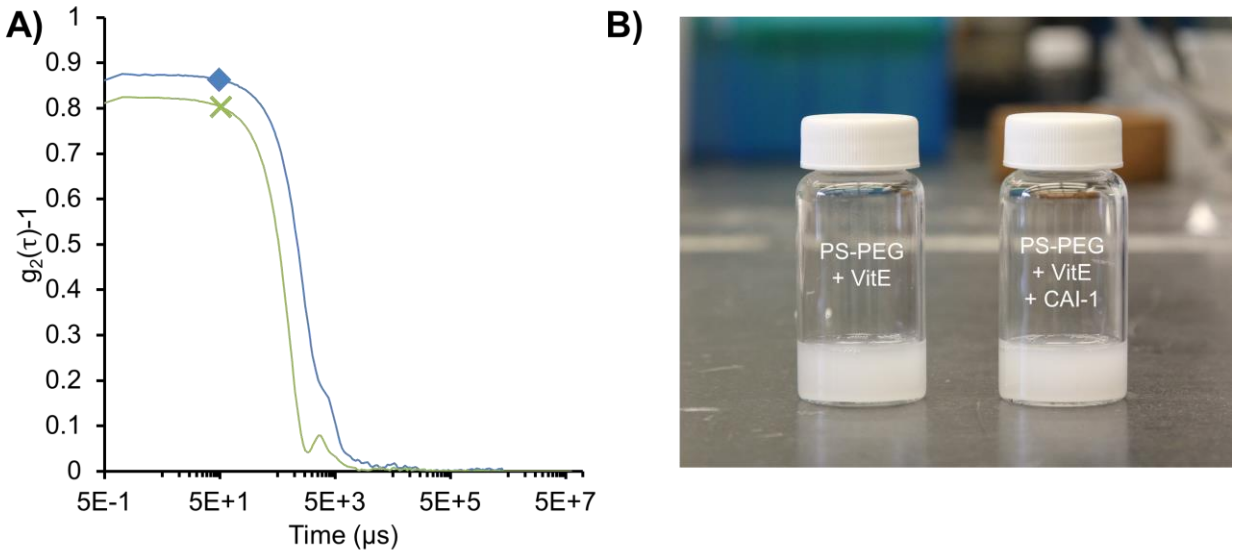

Figure S3. Dialysis precipitation of CAI-1 particles. (A) Dynamic light scattering correlation functions and (B) physical appearance of CAI-1 particles formed using slow dialysis precipitation with stabilizer, co-core, and CAI-1 (◆); and of VitE particles formed using slow dialysis precipitation with stabilizer and co-core (×).

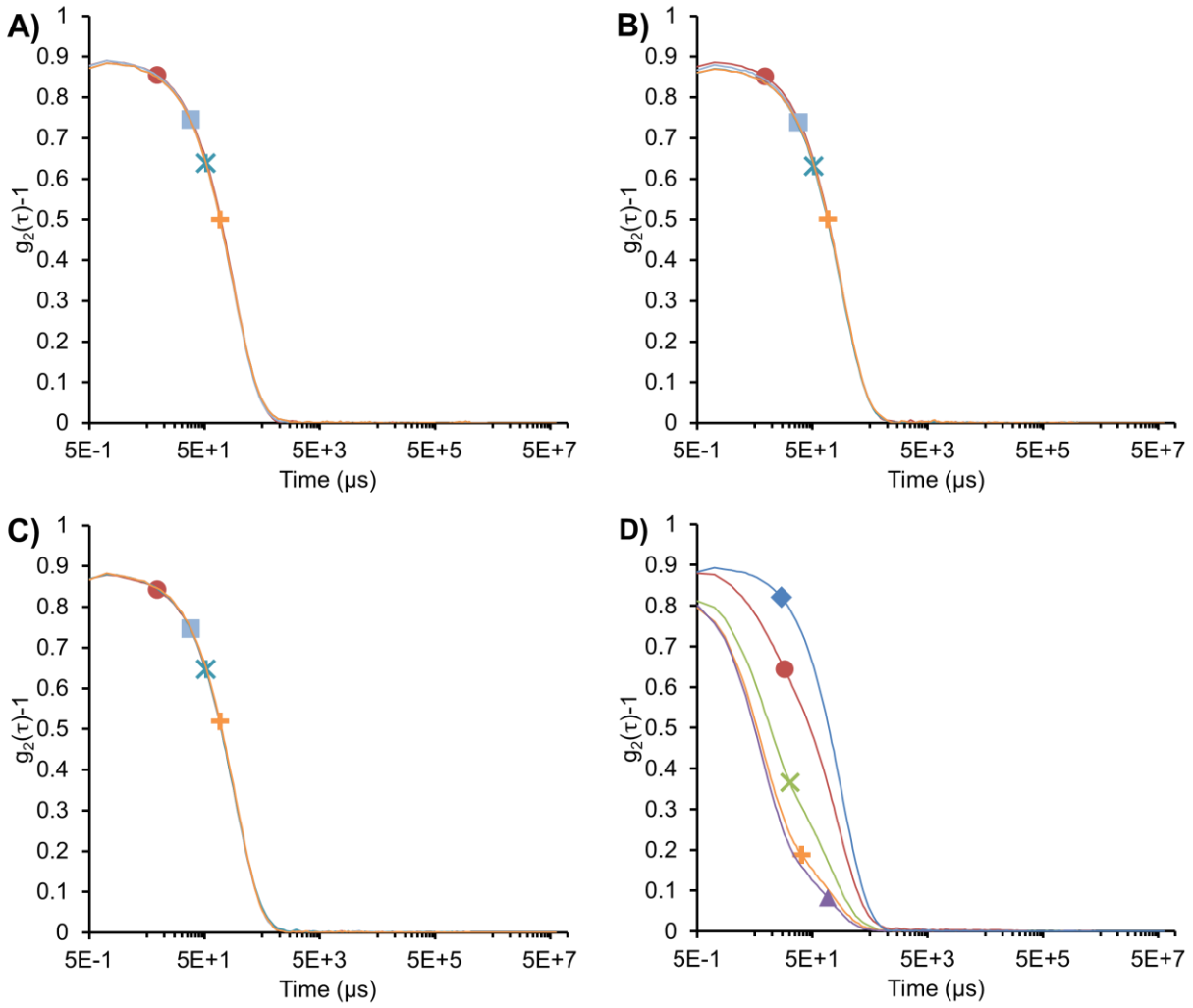

Figure S4. Stability of CAI-1 nanoparticles. Dynamic light scattering correlation functions of CAI-1 NPs following incubation in (A) PBS, (B) pH 2 PBS, and (C) LB medium at three minutes (●), one day (■), two days (✱), and three days (+). (D) Size distributions of CAI-1 NPs prior to incubation (◆) and incubation in 2% bile salts at 37°C at three minutes (●), thirty minutes (×), three hours (▲), and three days (+).

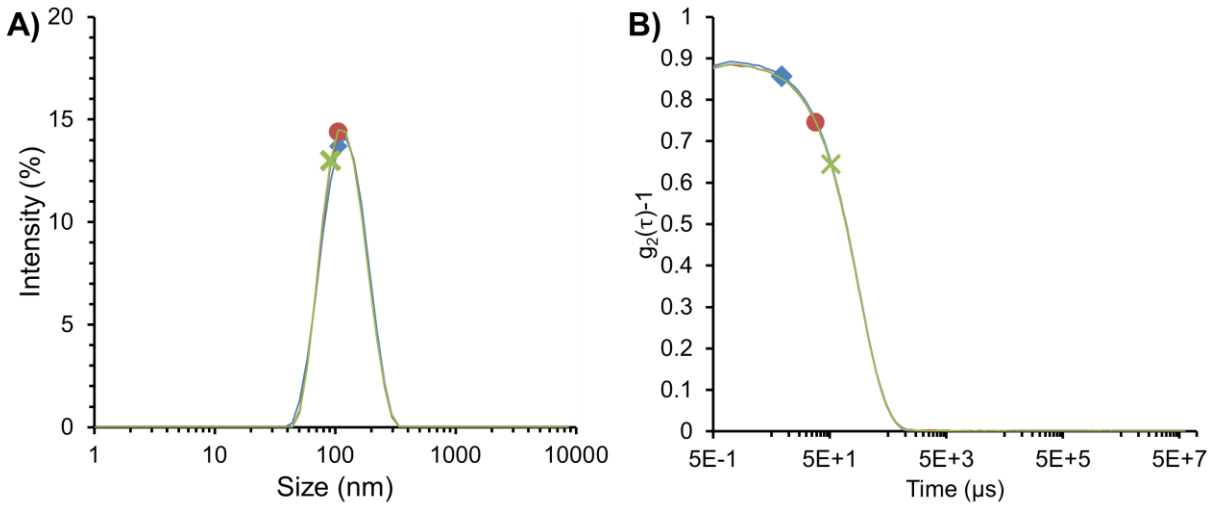

Figure S5. Stability of CAI-1 NPs following dialysis. Dynamic light scattering (A) size distributions and (B) correlation functions of CAI-1 NPs prior to dialysis (◆), and after dialysis in excess PBS for three (●) or eighteen hours (×).

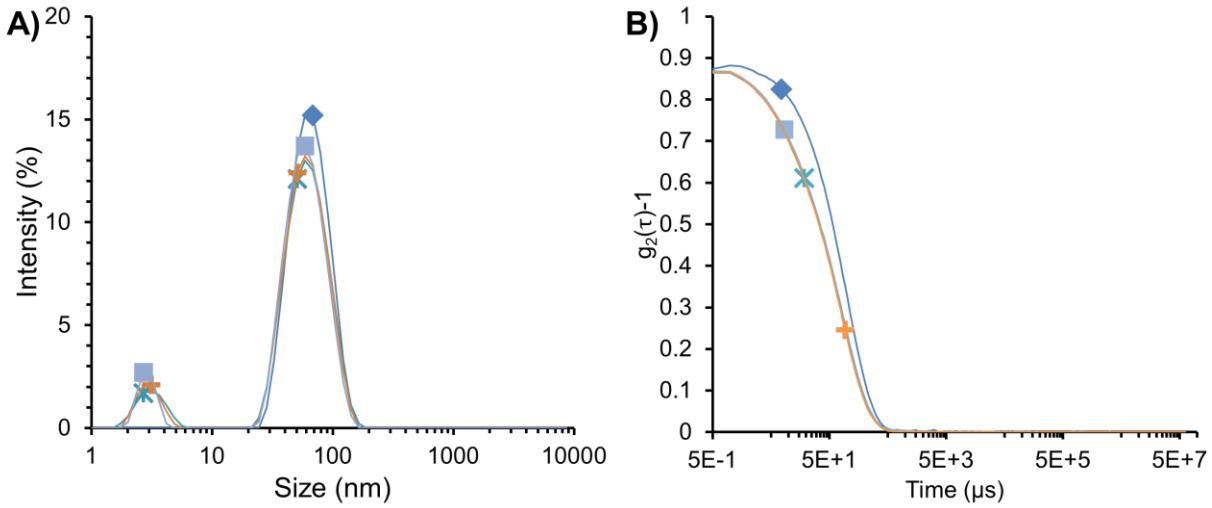

Figure S6. Stability of VitE NPs in bile salts. Dynamic light scattering (A) size distributions of and (B) correlation functions of VitE NPs prior to (◆), and after incubation in 2% bile salts at 37°C for one day (■), two days (✱), and three days (+).

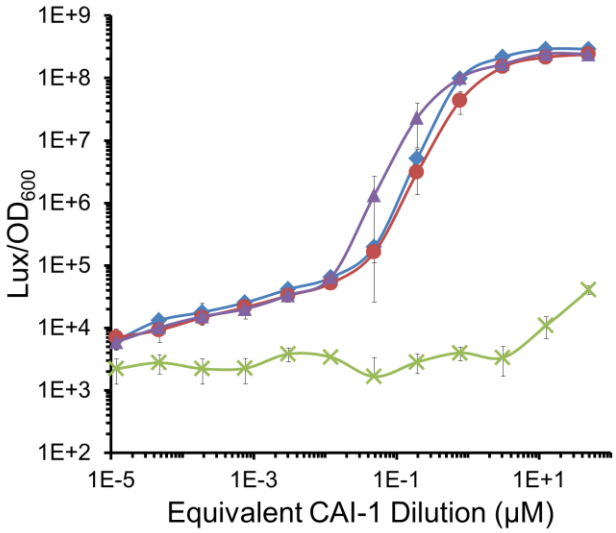

Figure S7. Bioactivity of separated CAI-1 NPs and nanoparticle-free solutions. Bioluminescence response of *V. cholerae* WN1102 following incubation with different amounts of CAI-1 NPs retained after ultrafiltration (◆), nanoparticle free CAI-1 NP ultrafiltration flow through (✕), dialyzed CAI-1 NPs (▲), and CAI-1 in DMSO (●). Activity was retained in nanoparticle fractions. Values are averages and error bars are standard deviations of three separate measurements.

Supplementary Tables

Formulation	Stabilizer		Physical co-core		Active Core		Nanoparticle Properties	
	Block copolymer	Conc (mg/mL)	Filler	Conc (mg/mL)	Drug	Conc (mg/mL)	Diameter (nm)	PDI
1	$PS_{1.6k}$-b-PEG_{5k}	10	-	-	-	-	22 ± 3.1	0.31 ± .033
2	$PS_{1.6k}$-b-PEG_{5k}	10	VitE	7.5	-	-	65 ± 0.22	0.08 ± .009
3	$PS_{1.6k}$-b-PEG_{5k}	10	VitE	7.5	CAI-1	7.5	112 ± 1.7	0.12 ± .009

Table S1. Summary of nanoparticle formulations and sizes. Reported nanoparticle sizes and polydispersities are averages of four measurements, and errors are standard deviations from four measurements.

Sample	Nanoparticle Properties			Effective diffusivity$_{(t=1\ s)}$ ($\mu m^2\ s^{-1}$)	
	Diameter (nm)	PDI	Zeta Potential (mV)	Simulated fluid	Intestinal mucus
Ettp5 CAI-1 NPs	107 ± 0.81	0.13 ± .01	-1.73 ± 7.02	1.25 ± 0.13	0.044 ± 0.026

Table S2. Summary of nanoparticle diffusivity. Reported nanoparticle sizes, polydispersities, and zeta potentials are averages of three measurements, and errors are standard deviations from three measurements. Reported effective diffusivities are geometric means, and errors are geometric standard deviations from three particle tracking experiments. Diffusivities are calculated at one second timescales. The <MSD> at a time scale of 1 s for Ettp5 CAI-1 NPs in mouse small intestine mucus was 29-fold lower than that of the same particles in simulated intestinal fluid.

References

1. Johnson, B. K.; Prud'homme, R. K. *AIChE J.* **2003,** 49, 2264-2282.
2. Higgins, D. A.; Pomianek, M. E.; Kraml, C. M.; Taylor, R. K.; Semmelhack, M. F.; Bassler, B. L. *Nature* **2007,** 450, 883-886.
3. Perez, L. J.; Karagounis, T. K.; Hurley, A.; Bassler, B. L.; Semmelhack, M. F. *Chem. Sci.* **2013,** 5, 151-155.
4. O'Toole, G. A. *J. Vis. Exp.* **2011,** 47, e2437
5. Pansare, V. J.; Bruzek, M. J.; Adamson, D. H.; Anthony, J.; Prud'homme, R. K. *Mol. Imaging Biol.* **2014,** 16, 180-188.
6. Ensign, L. M.; Henning, A.; Schneider, C. S.; Maisel, K.; Wang, Y.-Y.; Porosoff, M. D.; Cone, R.; Hanes, J. *Mol. Pharm.* **2013,** 10, 2176-2182.
7. Schuster, B. S.; Kim, A. J.; Kays, J. C.; Kanzawa, M. M.; Guggino, W. B.; Boyle, M. P.; Rowe, S. M.; Muzyczka, N.; Suk, J. S.; Hanes, J. *Mol. Ther.* **2014,** 22, 1484-1493.
8. Suh, J.; Dawson, M.; Hanes, J. *Adv. Drug Deliv. Rev.* **2005,** 57, 63-78.
9. Hammer, B. K.; Bassler, B. L. *Mol. Microbiol.* **2003,** 50, 101-104.
10. Lenz, D. H.; Mok, K. C.; Lilley, B. N.; Kulkarni, R. V.; Wingreen, N. S.; Bassler, B. L. *Cell* **2004,** 118, 69-82.
11. Miller, M. B.; Skorupski, K.; Lenz, D. H.; Taylor, R. K.; Bassler, B. L. *Cell* **2002,** 110, 303-314.
12. Waters, C. M.; Bassler, B. L. *Annu. Rev. Cell Dev. Biol.* **2005,** 21, 319-346.
13. Zhu, J.; Miller, M. B.; Vance, R. E.; Dziejman, M.; Bassler, B. L.; Mekalanos, J. J. *Proc. Natl. Acad. Sci.* **2002,** 99, 3129-3134.
14. Ng, W.-L.; Perez, L.; Cong, J.; Semmelhack, M. F.; Bassler, B. L. *PLoS Pathog.* **2012,** 8, e1002767